

Magnetism, structure, and charge at the Mott-Hubbard insulator-metal transition in pure NiS₂

Yejun Feng,^{1,2} R. Jaramillo,³ A. Banerjee,² J. M. Honig,⁴ and T. F. Rosenbaum²

¹*The Advanced Photon Source, Argonne National Laboratory, Argonne, IL 60439, USA*

²*The James Franck Institute and Department of Physics,
The University of Chicago, Chicago, IL 60637, USA*

³*School of Engineering and Applied Science, Harvard University, Cambridge, MA 01238, USA*

⁴*Department of Chemistry, Purdue University, West Lafayette, IN 47907, USA*

We use synchrotron x-ray diffraction and diamond anvil cell techniques to probe both the magnetism and the structure of single crystal NiS₂ across its Mott-Hubbard transition. In the insulator, the low-temperature antiferromagnetic order results from superexchange among correlated electrons and couples to a (1/2, 1/2, 1/2) superlattice distortion. Applying pressure suppresses the insulating state, but enhances the magnetism as the superexchange increases with decreasing lattice constant. The dependence of the magnetism on the lattice constant is robust for band filling as well as for band broadening. Under pressure, the lattice symmetry is reduced by a monoclinic distortion in the metal, pointing to the primary influence of charge correlations at the transition. There exists a wide regime of phase separation that may be a general characteristic of correlated quantum matter.

PACS numbers: 71.30.+h, 75.30.Kz, 61.05.cp, 64.75.Qr

One of the great challenges of understanding correlated materials is teasing apart the relative influences of the spin, charge, orbital, and lattice degrees of freedom. The point where an insulator becomes a metal highlights acutely the competition between mechanisms, but it also affords a special opportunity to limn the pertinent physics when different routes across the phase transition are available. Going back to the original ideas of Mott and Hubbard, we know that strong Coulomb repulsion between electrons on a single lattice site can localize charge even when band theory predicts metallic behavior [1–3]. At the same time, Slater claimed that antiferromagnetism alone could account for the formation of the insulating gap [4]. Anderson attributed antiferromagnetism to a consequence of superexchange between electrons that are localized by correlation [5]. All can be subsumed by symmetry changes wrought by a structural phase transition [6].

We use synchrotron x-ray diffraction in a diamond anvil cell to parse the roles of the low temperature antiferromagnetism and the lattice structure, both through the insulating state and at the transition to the metal in the Mott-Hubbard system, NiS₂. The reduced symmetry in the metal to monoclinic - a highly unusual occurrence for correlated materials described below - eliminates the change in the structure as a likely origin of the delocalization of charge. By comparison of the pressure-induced transition in the pure compound to the insulator-metal transition (IMT) driven by chemical substitution of Se for S, we identify the charge degrees of freedom as the predominant driving mechanism. Realizing the IMT in high quality single crystals of a stoichiometric material using applied pressure further clarifies the physics by avoiding complications that arise from chemical disorder, most notably the competition between Anderson localization and

the Mott transition.

The cubic pyrite NiS₂ has been long recognized as a canonical Mott-Hubbard correlated insulator [7–9]. Band structure calculations put the S 3*p* band and Ni *t*_{2*g*} band well below the half filled Ni *e*_{*g*} band, pointing to on-site Coulomb repulsion as the source of the insulating energy gap [10], which lies in the range 1-10 meV [11]. The small size of this gap demonstrates that NiS₂ is an incipient Mott insulator [12] with the Coulomb repulsion *U* comparable to the *e*_{*g*} bandwidth, *W* = 2.1 eV [10]. The gap can be suppressed either by Se doping [13–16] or applied pressure [7, 17–19]. Doping with Se expands the lattice and reduces the Ni 3*d* bandwidth, and the IMT is thought to be driven by increasing charge transfer between the Ni 3*d* and Se 4*p* bands [7]. Pressure directly tunes the ratio *U/W* and provides a more direct approach to the Mott-Hubbard model.

The ground state of NiS₂ exhibits two coexisting antiferromagnetic structures at ambient pressure [8]. M1 has a (1, 0, 0) wavevector and emerges from a second order phase transition at *T*_{N1} = 37 to 54 K, where the transition temperature depends on S vacancy concentration and varies from sample to sample (*i.e.* Ref. [8]). M2 has a (1/2, 1/2, 1/2) wavevector and emerges from a first-order phase transition at *T*_{N2} = 30 ± 1 K, with a transition temperature that is consistent across all published reports and materials. Similar coexistence of M1 and M2 antiferromagnetism is observed in CoO, where both emerge at a single transition temperature and are each responsible for a particular magnetostriction [20]. In NiS₂, however, M1 and M2 emerge at different temperatures and M1 is not coupled to the lattice [21, 22]. The magnetostrictive response to M2 is likely rhombohedral [21]. However, the distortion from cubic symmetry is extremely small, with a relative lattice constant dis-

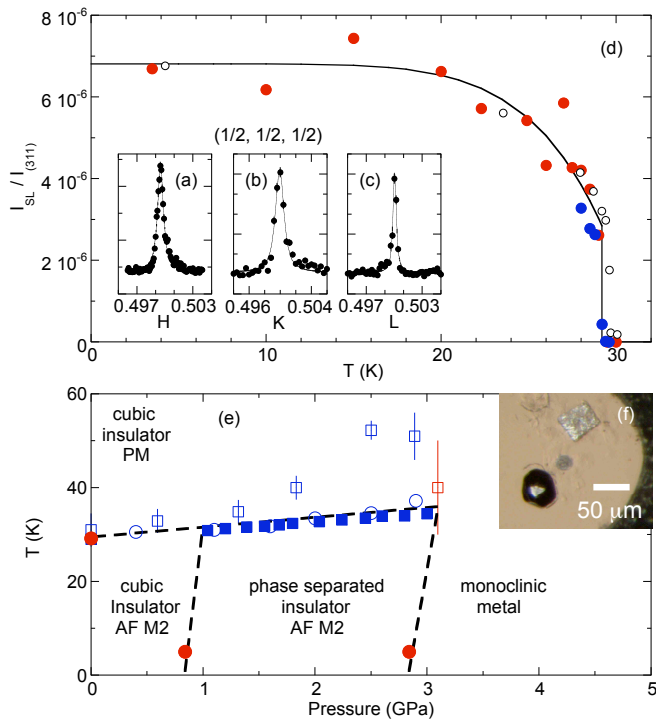


FIG. 1: (color online). (a-c): H, K, L scans of $(1/2, 1/2, 1/2)$ superlattice diffraction at ambient P and $T = 5.8$ K. (d) Superlattice intensity I_{SL} at ambient P plotted as a function of temperature. I_{SL} is averaged over $(3.5, 1.5, 1.5)$, $(3.5, 0.5, 1.5)$, $(2.5, 1.5, 1.5)$, and $(2.5, 0.5, 1.5)$, and normalized to $(3, 1, 1)$. Data were taken while warming (red) and cooling (blue) through $T_{N2} = 29.2$ K. The intensity of magnetic neutron diffraction from the $(1/2, 1/2, 1/2)$ M2 magnetic order (open circles, data from Ref. [8]) scales linearly to the x-ray superlattice intensity. Solid line is a guide to the eye. (e) P - T phase diagram of pure NiS_2 . T_{N2} is taken from Refs. [18, 19] (blue open symbols) and our transport measurements [24] (blue solid squares). Our x-ray measurements (red solid circles) are plotted together with the IMT determined by transport (red open square, [19]). M2 magnetism disappears above 2.84 GPa at $T = 5$ K. The high P phase is monoclinic. There is a wide region between 0.85 and 2.84 GPa where the two phases are separated in space but coexist. Dashed lines mark the estimated phase boundaries. (f) Micrograph of the pressure chamber including single crystal NiS_2 . Ruby and silver serve as manometers at room T and low T , respectively.

tortion $\Delta a/a < 2 \times 10^{-4}$ [22], and for our diffraction measurements we model the ground state using a cubic matrix.

We carried out high pressure single-crystal x-ray diffraction at beamlines 4-ID-D and 6-ID-B of the Advanced Photon Source. In a vertical scattering geometry with a psi-diffractometer, the detector slits were 50 μm wide and 1.3 m away from the sample along the 2θ arm in order to achieve a high q -resolution (FWHM $1 \times 10^{-3} \text{\AA}^{-1}$) for 20 keV x-rays [23]. The use of double-

bounce Pd mirrors and an energy discriminating NaI scintillation detector eliminated higher-harmonic contamination of the diffraction signal. Our single crystals were grown by the Te flux method to remove potential complications from excess impurity concentrations [14], with 25 to 50 μm diameters that fit well within the pressure chamber of a diamond anvil cell (Fig. 1). We estimate our sample stoichiometry as $\text{NiS}_{1.96}$ from the measured lattice constants and resistivity [9]. Five different crystals were studied under pressure using a methanol:ethanol 4:1 mixture for the pressure medium. Pressure P at base temperatures from $T = 3.5$ to 5.8 K was calibrated in situ using silver diffraction [23].

At ambient pressure and $T < T_{N2}$ we discover charge-originated superlattice diffraction peaks at every $(1/2, 1/2, 1/2)$ -type position in reciprocal space (Fig. 1a-c), corresponding to the low- T M2 magnetic structure. We demonstrate in Fig. 1d that the temperature dependence of the superlattice intensity scales linearly with the magnetic M2 neutron diffraction intensity [8]. These observations point to a spin-Peierls type coupling between the M2 antiferromagnetic order and the crystal lattice, which is in addition to the magnetostriction. The intensity of the superlattice peaks provides a quantitative estimate of lattice distortion δ through the relation $I_{SL}/I_{(311)} = |\mathbf{q} \cdot \delta/2|^2 S(SL)/S(311)$, where \mathbf{q} is the superlattice ordering wavevector and $S(SL)$ and $S(311)$ are the atomic form factors at the superlattice and $(3, 1, 1)$ positions, respectively. Given the domain degeneracy in each superlattice order and uncertainty over the direction of superlattice displacement δ , we evaluate $|\mathbf{q} \cdot \delta/2|^2$ by averaging the direction of δ uniformly over the full 4π solid angle. Further averaging was carried out over four superlattice orders (Fig. 1d). In this way we estimate $\delta = 2.3 \pm 0.7 \times 10^{-3} \text{\AA}$, which is a factor of 4×10^{-4} smaller than the lattice constant.

Using the superlattice reflections as a measure of the M2 order, we are able to track the magnetism and the crystal lattice through the pressure-driven IMT. The P - T phase diagram is summarized in Fig. 1e. The M2 phase boundary has been measured by several groups [18, 19, 24]. The only existing magnetic scattering study [18] was limited to $P < 2.9$ GPa and placed the IMT phase boundary at 1.3 ± 0.4 GPa by identifying it with a possible lattice discontinuity, leading to the conclusion that the magnetism is continuous across the IMT. Here we observe the $(1/2, 1/2, 1/2)$ -type superlattice distortion at every pressure from 0 to 2.84 GPa (Fig. 2a-d) at base temperature. Above 2.84 GPa the superlattice vanishes in all samples (Fig. 2e-f). A review of published accounts of the IMT phase boundary [17, 19] places the critical pressure in the range 2.2 - 3.1 GPa. This range brackets the upper limit of the observed superlattice diffraction. It is therefore natural to conclude that the disappearance of the low-temperature M2 magnetic state, the structural phase transition, and the IMT all

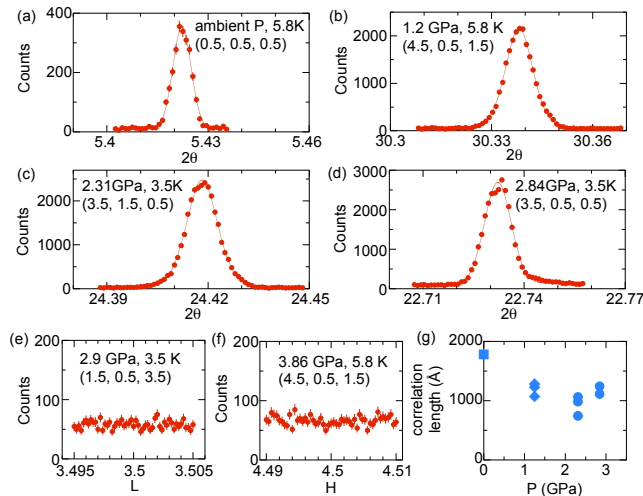


FIG. 2: (color online). (a-d) Longitudinal scans of the superlattice at four pressures between 0 and 2.84 GPa. All lineshapes are nearly resolution limited, indicating that the crystal remains cubic throughout the insulating phase with long M2 correlation lengths (see text). (e, f) Null scans through the superlattice positions at 2.90 ± 0.05 and 3.86 ± 0.12 GPa. (g) Calculated lower bounds of correlation lengths for superlattice domains directly inverted from the lineshape width. Points at each P represent scans through different superlattice orders.

coincide at $P \sim 2.9$ GPa.

High-resolution θ - 2θ longitudinal scans at all orders of the superlattice reflection are consistently close to resolution-limited (Fig. 2a-d), testifying to M2 correlation lengths greater than 1000 Å (Fig. 2g). This length is consistent for all pressures within the phase boundary. For the fcc lattice peaks the longitudinal scans (Fig. 3) reveal a more complicated picture. All measured lineshapes are resolution-limited for $0 < P < 0.85$ GPa. However, beginning at 0.85 GPa, we observe multiple splitting of diffraction peaks in almost every sample at every pressure (Fig. 3). This indicates the emergence of structural domains of reduced symmetry. Importantly, the superlattice reflections remain resolution limited before disappearing entirely above 2.84 GPa (Fig. 2). The contrast between the multiply-split fcc Bragg peaks and the sharp superlattice reflections is proof of phase coexistence between 0.85 GPa and 2.84 GPa. Phase coexistence over such a wide range suggests that the effect of pressure on the free energy of the insulator is gradual, and that the free energy difference between the insulating and metallic states is very small. We note that the onset of the high-pressure structural phase that we observe at 0.85 GPa may explain the phase boundary at 1.3 ± 0.4 GPa claimed in previous neutron scattering work [18].

The crystal symmetry of the high-pressure metallic phase can be determined either with single crystal refinement of a single-domain specimen or with powder

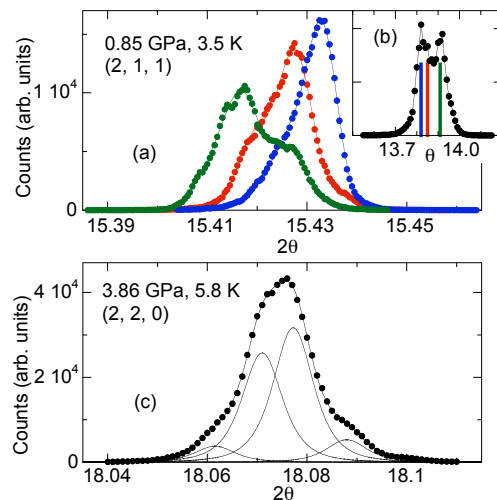


FIG. 3: (color online). (a) Longitudinal θ - 2θ scans of the (2, 1, 1) lattice reflection at 0.85 ± 0.10 GPa, the lowest P at which phase separation was observed. (b) Rocking curve recorded at the same (2,1,1) reflection. The colored bars indicate the three different central θ values used in the scans in panel (a). (c) Longitudinal scan of the (2, 2, 0) lattice reflection at 3.86 GPa where only the high P phase is present. The four-fold splitting of (2, 2, 0) requires lattice symmetry of monoclinic or lower.

refinement of a polycrystalline sample with full knowledge of symmetry split peaks. We identified a single-domain sample in the high pressure phase at 2.9 GPa. Six diffraction orders were measured and a least-squares fit reveals a largely-monoclinic structure with lattice parameters $a = 5.585$ Å, $b = c = 5.602$ Å, $\alpha = \gamma = 89.98^\circ$, $\beta = 89.93^\circ$ (Fig. 4a). The values of $(a - c)/a$ and $(90^\circ - \beta)$ measured at $P = 2.9$ GPa are consistent with measurements at 3.86 GPa (Fig. 3c), where the four-fold splitting of the (220) peak only can be explained by a symmetry of monoclinic or lower. Constraining the symmetry to monoclinic, we obtain $a = 5.576$ Å, $b = c = 5.585$ Å, $\beta = 89.945^\circ$ at 3.86 GPa (Fig. 4a). The four-fold splitting of (2, 1, 1) at 0.85 GPa (Fig. 3a) is consistent with this picture, as it cannot be explained by a single phase of symmetry higher than monoclinic. Notably, symmetry reduction on passing into the metallic phase is the opposite of what is observed in many other transition metal oxides, including the prototypical Mott-Hubbard system, V_2O_3 , which is a rhombohedral metal and a monoclinic insulator. For a non-interacting bandstructure, a reduction of lattice symmetry favors insulating behavior [6]. The observation here for NiS_2 that the symmetry is reduced in the metal therefore emphasizes the role played by electron correlations in the insulator.

The connection between the correlated Mott-Hubbard insulator and M2 antiferromagnetism is revealed by plotting T_{N2} as a function of lattice constant for both NiS_2 under pressure and $NiS_{2-x}Se_x$ (Fig. 4b). Antiferromag-

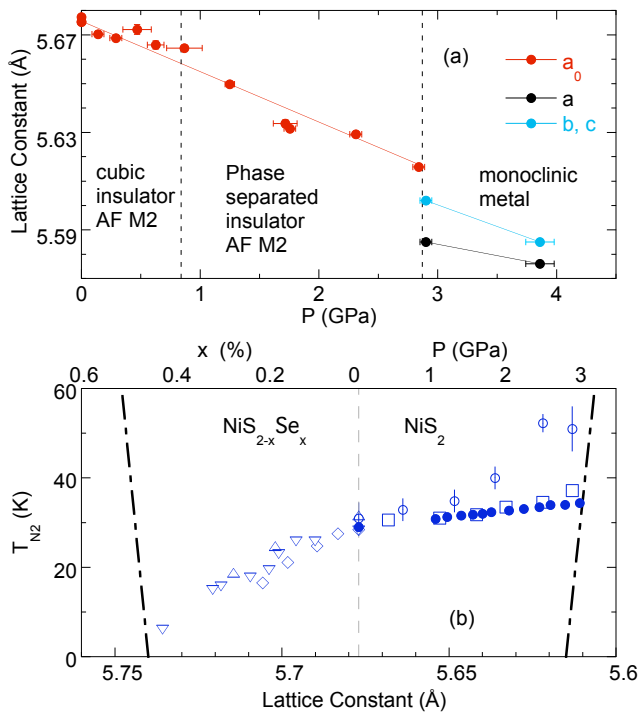


FIG. 4: (color online). (a) Lattice constants vs. pressure for NiS_2 at $T = 5$ K. Both the low P and high P phases were observed in the phase separated region, but with insufficient detail to determine the lattice parameters of the high P phase. The lattice constants of the low P phase were determined from the d -spacings of both the superlattice and cubic fcc reflections. (b) T_{N2} as a function of low temperature lattice constant for both NiS_2 under pressure and $\text{NiS}_{2-x}\text{Se}_x$ (open symbols: Ref. [13, 18, 19]; solid circle, [24]). The two dot-dash lines mark the first-order boundaries of the IMT driven by pressure and chemical substitution, and bound the M2 order.

netic coupling of correlated electrons results from superexchange through the S ligand fields [5]. This coupling grows stronger as the lattice constant is reduced [2], whether by chemical substitution or by external compression. For the NiS_2 system, T_{N2} increases as the lattice constant shrinks (Fig. 4b), consistent with the superexchange interaction. The M2 phase only vanishes when the local moments disappear in the high pressure metallic state. M2 therefore should be considered as a byproduct of electron correlation and is not by itself responsible for driving the insulating state. Important evidence for this also comes from resistivity measurements which show that the Arrhenius activation energy is unchanged on cooling through T_{N2} at ambient P . Hence the insulating energy gap is well established before the formation of the M2 phase [11, 24].

Our results address the longstanding debate over the role of magnetism at the IMT [25], while at the same time raising questions about quantum phase transitions

in the presence of strong electron correlations. The broad regime of phase coexistence that we observe while tuning U/W adds to a growing list of correlated electron systems that exhibit phase coexistence around a first order quantum phase transition [26, 27]. More generally, according to Luttinger's theorem the volume enclosed by the Fermi surface is unaffected by electron-electron interaction to all orders of perturbation theory [2, 3, 28]. The question of whether Luttinger's theorem holds until the point where the Fermi surface is destroyed by correlation is the subject of much debate, most notably in the field of high- T_c superconductivity in which the Mott-insulating parent state appears to develop a Fermi surface as it is tuned towards optimal doping [29]. Our results show that the correlated phase in NiS_2 always exhibits M2 antiferromagnetism and a superlattice distortion. Therefore, while the superexchange interaction is not itself responsible for the electron localization it may play an important role in precluding the existence of a Fermi surface in the low pressure phase.

We are grateful to D. Robinson and J.-W. Kim for technical support at 6-ID-B and to X. Yao for growth of the crystals. The work at the University of Chicago was supported by NSF Grant No. DMR-0907025. Use of the Advanced Photon Source was supported by the U.S. DOE-BES, under Contract No. NEAC02-06CH11357.

-
- [1] N. F. Mott, Proc. Phys. Soc. London A **62**, 416 (1949); J. Hubbard, Proc. R. Soc. London A **281**, 401 (1964).
 - [2] N. F. Mott and Z. Zinamon, Rep. Prog. Phys. **33**, 881 (1970).
 - [3] M. Imada, A. Fujimori, and Y. Tokura, Rev. Mod. Phys. **70**, 1039 (1998).
 - [4] J. C. Slater, Phys. Rev. **82**, 538 (1951); T. Moriya and K. Ueda, Rep. Prog. Phys. **66**, 1299 (2003).
 - [5] P. W. Anderson, Phys. Rev. **115**, 2 (1959).
 - [6] D. Adler, Rev. Mod. Phys. **40**, 714 (1968).
 - [7] J. A. Wilson and G. D. Pitt, Philo. Mag. **23**, 1297 (1971).
 - [8] T. Miyadai *et al.*, J. Phys. Soc. Jap. **38**, 115 (1975).
 - [9] G. Krill *et al.*, J. Phys. C **9**, 761 (1976).
 - [10] D. W. Bullett, J. Phys. C **15**, 6163 (1982).
 - [11] R. L. Kautz, M. S. Dresselhaus, D. Adler, A. Linz, Phys. Rev. B **6**, 2078 (1972).
 - [12] Q. Si, E. Abrahams, J. Dai, and J.-X. Zhu, New J. Phys. **11**, 045001 (2009).
 - [13] S. Sudo, J. Mag. Mag. Mat. **114**, 57 (1992); H. S. Jarrett *et al.*, Mat. Res. Bull. **8**, 877 (1973).
 - [14] X. Yao *et al.*, Phys. Rev. B **54**, 17469 (1996); J.M. Honig and J. Spalek, Chem. Mater. **10**, 2910 (1998).
 - [15] A. Y. Matsuura *et al.*, Phys. Rev. B **53**, R7584 (1996).
 - [16] A. Husmann *et al.*, Science **274**, 1874 (1996).
 - [17] Y. Sekine *et al.*, Physica B **237**, 148 (1997); N. Takeshita *et al.*, arXiv:0704.0591 (2007).
 - [18] P. Panissod, G. Krill, C. Vettier, and R. Madar, Solid State Comm. **29**, 67 (1979).
 - [19] N. Mori and H. Takahashi, J. Mag. Mag. Mat. **31**, 335 (1983).

- [20] W. Jauch *et al.*, Phys. Rev. B **64**, 052102 (2001); K. Tomiyasu, T. Inami, and N. Ikeda, Phys. Rev. B **70**, 184411 (2004).
- [21] T. Thio, J. W. Bennett, and T. R. Thurston, Phys. Rev. B **52**, 3555 (1995).
- [22] H. Nagata, H. Ito, and T. Miyadai, J. Phys. Soc. Jap. **41**, 444 (1976).
- [23] Y. Feng *et al.*, Rev. Sci. Instrum. **81**, in press (2010).
- [24] A. Banerjee *et al.*, to be published.
- [25] J. Spalek *et al.*, Phys. Rev. B **78**, 100401 (2008).
- [26] Y. J. Uemura *et al.*, Nature Phys. **3**, 29 (2007).
- [27] M. M. Qazilbash *et al.*, Science **318**, 1750 (2007).
- [28] M. Oshikawa, Phys. Rev. Lett. **84**, 3370 (2000).
- [29] N. Doiron-Leyraud *et al.*, Nature **447**, 565 (2007).